Natural Hazards
and Earth System
Sciences
Discussions

1 # An atmospheric approach to the flood disaster in the Western
2 # Black Sea region (Turkey) on 10-12 August 2021

3 **Onur Halis[1], Barbaros Gönençgil[2], Zahide Acar[3]**

4 [1]Geography Department, Istanbul University, Istanbul, 34000, Turkey.

5 [2]Geography Department, Istanbul University, Istanbul, 34000, Turkey.

6 [3]Geography Department, Çanakkale Onsekiz Mart University, Canakkale, 17000, Turkey.

7 Correspondence to: Onur Halis (onurhalis@istanbul.edu.tr)

8 **Abstract**. Precipitation is one of the important climate elements that directly affect disasters with its high spatial and
9 temporal variability. In addition to the changes in precipitation amounts between years, precipitation intensity and
10 duration are also necessary for precipitation climatology. The Black Sea coast is one of the regions that attract attention
11 in terms of precipitation amounts, intensity and duration in the world. Countries bordering the Black Sea have been
12 struggling with flash floods, which have arisen due to excessive rainfall in recent years. The flood has had the most
13 loss of life and devastating effect in recent times, especially in the summer season, which occurred after heavy rains
14 on August 10-12, 2021. In this disaster, 82 people lost their lives due to the flood. In addition, the flood damaged
15 energy, transportation, access to drinking water, communication, and shelter areas. From 10 to August 12, total
16 accumulated rainfall amounts of 452.5, 389.2, 386.2 and 281.1 mm were measured in the Bozkurt Mamatlar Village,
17 Devrekani Kuzköy, Küre and Abana settlements of Kastamonu city, respectively. Additionally, precipitation was
18 recorded 235.9 mm in Ulus Ceyüpler Village of Bartın, 317.9 mm in Ayancık and 225.8 mm in Türkeli of Sinop. In
19 this study, the atmospheric conditions of the flood disaster were examined. The Basra low pressure settled over the
20 eastern Black Sea during this period. On August 8-9, a trough developed above Anatolia at the level of 500 hPa. Due
21 to the low pressure remaining on the region, the system coming to the Black Sea Basin from the north turned towards
22 the east of the Black Sea as of August 8. Especially at this date, while high-pressure conditions continued in most
23 western parts of the Black Sea, the pressure falling from the Sevastopol-Kastamonu line to the east attracted the system
24 coming from the north. On August 10 2021, the surface temperature of the Black Sea, especially the eastern part,
25 reached 28.3 °C (3.5 °C higher than average). The temperature difference between sea surface temperatures and 850
26 hPa reached 13 °C degrees. These conditions resulted in a strong low-level moisture convergence development that
27 continued for three days in the Black Sea Basin. Thus, the developing convective cell gradually became more vigorous,
28 expanded its area of influence in the interior of the land due to the cyclone movement as of the morning of August 10
29 and caused heavy rains with the effect of the topography.

30

31

1 Introduction

33 Precipitation is one of the most variable elements of the climate and is controlled by factors such as geographical
34 location, general atmospheric circulation and local conditions (Erinç, 1996; Erol, 2011). In addition to these, it can be
35 said that the trends in extreme precipitation have a more sensitive response to climate change than other climate
36 elements. As a result of this situation, extreme climate events attract more attention (Katz & Brown, 1992). For
37 example, Bocheva et al. (2009), in their study covering the whole of Bulgaria, compared the total precipitation and
38 heavy precipitation in the two periods, 1961-1990 and 1991-2005 and found that a significant amount of daily heavy
39 precipitation was experienced in the second period. Especially in Bulgaria, due to heavy rains in 2005, 25 people died
40 their lives and caused more than 500 million Euros of damage.

41 Excessive rainfall and the mechanisms that cause this rainfall lead to disasters such as landslides and floods, causing
42 socio-economic problems and, most importantly loss of life. In particular, the rugged topography of the eastern part
43 of the Black Sea Basin, the suddenly rising mountains, and the interaction between the sea and the land has led to
44 increased rainfall and devastating floods in the countries bordering the Black Sea in recent years. For example, the
45 flood on 6-7 July 2012 in Krymsk, Novorossiysk and Glendzhik in the Krasnodar Region of Russia caused
46 approximately 170 deaths and USD 625 million in damage (Alexeevsky et al., 2016; Kapochkina et al., 2015). On
47 August 22, 2012, due to heavy rains in the northeast of the Black Sea, a flood occurred in the Tuapse region of Russia
48 (Alexeevsky et al., 2016). On June 20, 1988, 179 mm of precipitation in 4 hours and 50 minutes was measured in
49 Novorossiysk in the Krasnodar Region of Russia. It was stated that the water hose was also influential in this
50 precipitation (Alexeevsky et al., 2016; Kapochkina et al., 2015). In flood triggered by the development of the
51 convective cell in the Mediterranean cyclone, the total amount of precipitation on 24–25 October varied from 253 to
52 362 mm in the Tuapse River basin and 208.9 mm in the Shakhe River basin to 53.2 mm near the Sochi River mouth
53 and 83.6-112 mm in the Mzymta River basin (Korshenko et al., 2020). One of the countries affected by floods due to
54 heavy rains in this region is Turkey. Yüksek et al. (2013) examined 51 significant floods in the Eastern Black Sea
55 Basin of Turkey between 1955 and 2005 years, and they stated that 258 deaths occurred as a result of these floods;
56 the damage was close to the US $500,000,000. On August 24, 2015, located on Turkey's Eastern Black Sea coast, 136
57 mm in Hopa, 64 mm in Arhavi and 109 mm in precipitation in Borcka were measured. Eleven people lost their lives
58 in the flood, and the economic loss reached 1 million dollars (Baltaci, 2017). One of the most significant reasons for
59 this excessive rainfall is a positive anomaly of the sea surface temperature (SST) over the Black Sea (Baltaci, 2017;
60 Doğan et al., 2019). Extreme rains, the effect of which gradually increases in the summer seasons, have recently

61 caused more than one flood. In this study, we tried to examine the atmospheric conditions of the hourly and daily

62 precipitation totals that occurred on 10-12 August 2021 in the provinces of Sinop, Kastamonu and Bartın on the Black

63 Sea coast. Within the scope of the study, answers to the following questions were sought:

64 • If there is an increase in the number and severity of atmospheric originated floods on the Black Sea coast,
65 what factors cause this?
66 • How is the temperature gradient of the upper and lower atmospheres with the surface temperatures?
67 • What are the trends in changes in sea surface temperatures?
68 • What is the role of the gradually warming sea surface temperature in the Black Sea in heavy rains?

69 • What is the role of topography in the variation of precipitation intensity?

70 The answers to the above questions are essential in understanding and predicting the atmospheric mechanisms that

71 cause excessive precipitation in the Black Sea coast of Turkey.

72 2 Study Area

73 The provinces of Sinop, Kastamonu and Bartın, located in the Western Black Sea region of Turkey and stretch along

74 the Black Sea coast for 420 km, constitute the study area (Fig. 1). In these provinces, where approximately 800

75 thousand people live, there are many settlements in the river valleys (Turkish Statistical Institute, 2021). The fact that

76 the topographic relief does not show a homogeneous feature, suddenly changing altitude and slope conditions cause

77 uneven distribution of precipitation. Especially within 15 km of the coast, the altitude rises above 1000 meters. The

78 Küre Mountains, stretching between Bartın and Sinop and reaching a height of 2019 meters (Yaralıgöz Peak), are the

79 first mountain ranges in which the air masses coming from the Black Sea are forced to rise in a short distance. The

80 second mountain range to the south of these mountains, separated by plateaus and depressions, is the Ilgaz Mountains

81 at 2587 meters (Büyükhacat Hill). Most of the land within the study area, including these depressions and plateaus, is

82 above 1000 meters in elevation. When examined from a hydrological point of view, many short rivers take their source

83 from the Küre Mountains and flow into the Black Sea. The narrow and deep valleys opened by these rivers form

84 critical units in which the air masses are forced to rise by canalization and positively affect precipitation. This situation

85 played an essential role in the flood in the Bartın, Ezine and Ayancık Streams after extreme rains in the study area on
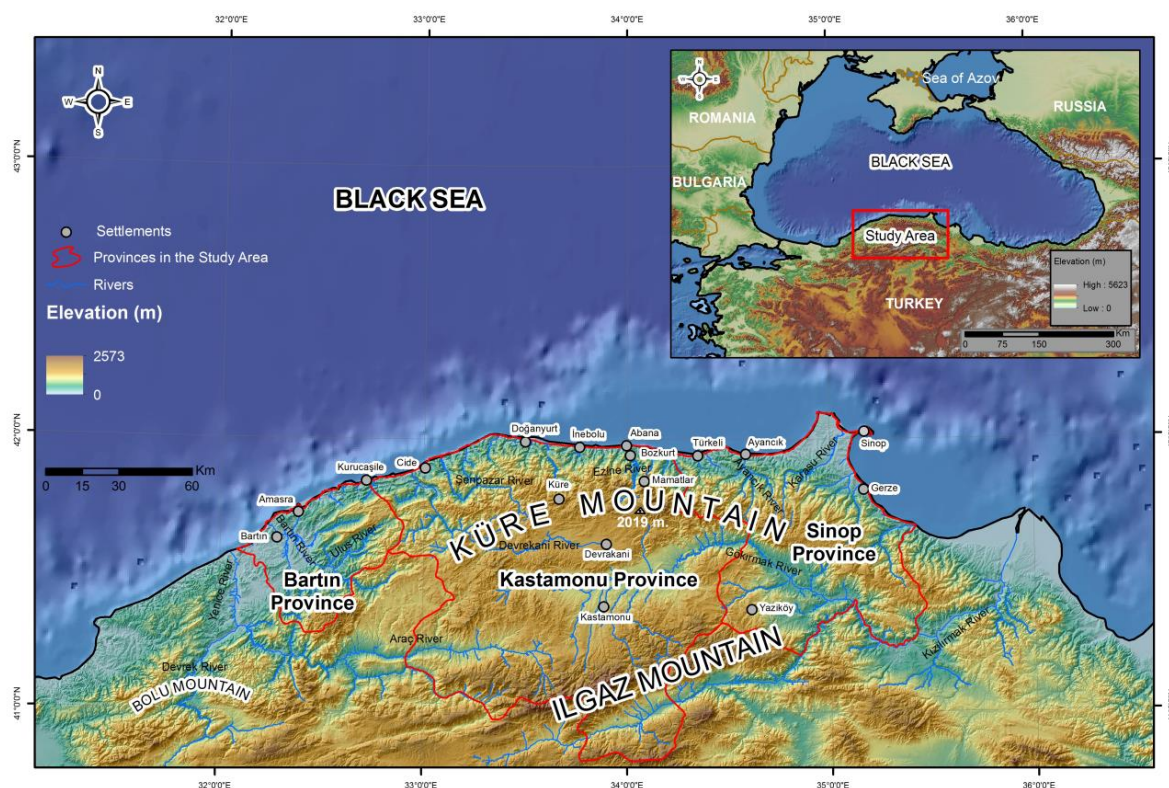
86 10-12 August.

Figure 1. Provincial borders constituting the study area, Western Black Sea Region.

3 Data and Method

In order to evaluate the extreme conditions in the study area, hourly and daily precipitation data of a total of 56 stations located in Sinop, Kastamonu and Bartın were used (Table 1, fig. 11, 12 and 13.). The ground charts, 850, 700 and 500 hPa synoptic maps used in the study were obtained from MGM (Turkish State Meteorological Service). In this study, long-term and daily NOAA High-Resolution Blended Analysis data from 1971-2000, 1991-2020 and 10-17 August 2021 were used to examine the role of sea surface temperatures in extreme precipitation (Reynolds et al., 2007). On 10-11-12 August 2021, Natural Color RGB, Day Microphysics RGB, Convection RGB data from Meteosat Second Generation were used to determine the spatial distribution of convective cells and to examine atmospheric conditions. In addition, SYNOP observations and NOAA's daily temperature data and 700 hPa u and v direction vector wind data were also used with these data.

101 **Table 1:** Description of the 56 meteorological stations included in the study and daily precipitation data. The stations marked with
102 a star were evaluated in terms of climatology.

No, Station Code and Name	Longitude (°E)	Latitude (°N)	Altitude (m)	10 Aug 2021 precipitation	11 Aug 2021 precipitation	12 Aug 2021 precipitation
1 19031 - Ağlı	33.55440	41.68440	1190	54.4	74.5	2.6
2 18215 - Araç	33.33060	41.24670	682	7.8	95.1	2.2
3 18705 - Araç Orman S.	33.35166	41.20388	1240	9.8	97.9	2.3
4 18514 - Azdavay	33.28360	41.63610	822	46.5	108.8	2.2
5 19032 - Mamatlar	34.12750	41.79470	1523	121.7	297.6	33.2
6 17604 – Cide*	32.94760	41.88220	42	2	40.4	5.4
7 17625 – Çatalzeytin*	34.21800	41.95380	9	73.2	6	0
8 18515 – Daday	33.43923	41.50068	1009	12.4	48.3	0.1
9 19030 - kuzköy	34.04420	41.77280	1436	93.4	262.7	33.1
10 17618 – Devrekani*	33.83450	41.59960	1099	50	92	0.6
11 18516 – Doğanyurt	33.45970	42.00670	7	25.5	1.3	6
12 18517 – İhsangazi	33.54060	41.21860	850	15.2	36.2	2
13 18704 – İncigez	33.48110	41.25860	1231	24.1	54.3	10
14 17024 – İnebolu*	33.76360	41.97890	49	12.4	34.8	24.6
15 18911 – İnebolu kar	33.71890	41.87470	960	115.9	137.4	21.7
16 18914 – Yolüstü	33.73366	41.91193	729	70	128.6	22.4
17 17074 – Kastamonu*	33.77560	41.37100	800	19.9	49	7.2
18 18706 – Başören	34.11720	41.29440	961	45.7	50.2	6.3
19 17606 – Bozkurt*	34.00370	41.95970	149	119.1	36.5	7.5
20 18997 - Mescit	33.89898	41.24982	1149	37.7	23	12.5
21 18513 – Pınarbaşı	33.12440	41.61780	644	56.9	92	2.2
22 18518 – Küre	33.71110	41.81060	1013	173.1	201.1	12
23 18520 – Seydiler	33.71860	41.62440	1052	49.9	55.9	0.4
24 18521 – Şenpazar	33.23000	41.81080	395	23.5	50.7	12.3
25 18522 – Taşköprü	34.22250	41.49420	632	41.3	48.6	3.3
26 17650 – Tosya*	41.01320	33.23000	860	23.6	14.6	0
27 19221 – Abana	34.00006	41.97741	9	122.6	141.7	16.8
28 19222 – Hanönu	34.50010	41.62828	430	36.8	74.1	10.1
29 18519- Pınarbaşı Kar	33.07890	41.55660	1019	15.9	72	7.4
30 17602 – Amasra	32.38270	41.75260	50	0	0	38.2
31 17020 – Bartın*	32.35690	41.62480	36	0	0	34.6
32 17721 - Bartın/Arıt	32.61560	41.68720	356	25.4	6.8	52.3
33 18692 - Hasankadı	32.47500	41.35140	1264	12.1	40.4	18.2
34 19007 - Kozcağız	32.34250	41.49440	51	0	24.9	34
35 18245 - Kurucaşile	32.73603	41.80513	126	3	1.4	30.1
36 17615 – Ulus*	32.63700	41.58190	182	57.6	71.6	21.6
37 19008 - Ulus/Ceyüpler	32.54420	41.47080	630	95.7	96.4	43.8
38 19009 - Ulus/Çubukeli	32.84940	41.69060	520	14.6	122.1	23.2
39 19207 – Kurucaşile	32.73603	41.80513	184	8.5	5.1	38.8
40 19039 – Ayancık	34.58110	41.92440	36	158.5	129.3	30.1
41 18546 - Akören	34.77140	41.83220	625	62.7	138	13.1

42	19040 - Çangal	34.65220	41.72060	1067	64.4	145.9	11.2
43	17620 – Boyabat*	34.78530	41.46300	347	20.2	70.6	2
44	18711- Dranaz	34.88530	41.62030	1109	32.1	71.5	6
45	19043 - Kavacık	34.58860	41.37830	1130	27.6	66.5	0.5
46	18547 – Dikmen	35.27250	41.66360	383	45.1	17.6	22.7
47	19042 - Dikmen	35.25390	41.53030	1003	42.5	17	3.5
48	18548 – Durağan	35.05060	41.43440	286	19.7	25.1	0
49	19041 - Durağan/Tekir	35.29810	41.34640	997	21.2	11.8	26.6
50	18136 – Erfelek	34.89470	41.87940	190	78.7	51.9	38.3
51	18549 – Gerze	35.17360	41.81190	87	65.2	10.3	61.1
52	18550 – Saraydüzü	34.84970	41.32850	422	4.8	47.9	0
53	17026 – Sinop*	35.15450	42.02990	29	111	10.6	32.8
54	18551 – Türkeli	34.33420	41.94110	123	82.1	143.7	0
55	19227- Sinop/Sarıkum	34.92277	42.02472	21	86	32.8	19.7
56	19229 - Sinop/Sazlı	34.87399	41.72357	1030	44.6	103.4	7

4 Findings

4.1 Synoptic Status

In terms of representing the general synoptic conditions of the study area, Karaca et al. (2000), as a result of the analysis of 15-year daily surface and 500 hPa synoptic maps, revealed that there are four main cyclone routes affecting Turkey (Fig. 2). The fact that especially the first two of these ways are effective on the Black Sea is vital in terms of the general synoptic conditions of the study area. The first of these originate in the southwest of Russia and passes over the Black Sea. The second originates from the Balkans and affects the Marmara and Black Sea Regions. These systems create intense precipitations throughout northern Turkey, effective in summer. Alexeevsky et al. (2016) also stated that the abnormal position in the northern location of the Azores anticyclone in recent years, with the movement of the anticyclone 1000-1500 km more north than usual, strong cyclogenesis from the Iberian Peninsula to the Balkans on the Mediterranean has become active. Thus the cyclones move from west to east along the Black Sea. In this study, meteorological conditions that caused flash floods in the provinces of Bartın, Kastamonu and Sinop on August 11 2021, were examined. In order to better understand the synoptic conditions of 10-12 August 2021, We started to evaluate the synoptic conditions of the day before the onset of heavy rains. When the synoptic situation at ground level is examined on August 9, it is seen that the Basra low pressure extends to the Eastern Black Sea Region (Fig. 3a). This situation created a low pressure over the entire Eastern Mediterranean, including Turkey. In the upper atmosphere, a ridge in the western Mediterranean and a trough developed over Turkey (Fig. 3b). In the 500 hPa meteorological maps, the winds developing following this trough formed northerly currents over the Western Black Sea and southerly currents over the Eastern Black Sea (Fig 4). In this case, the cold air entered from the northwest of the Black Sea. On August 10, the high-pressure area moved eastward over Europe and was located in the Northwest of the Black Sea (Fig. 3c). The blocking presence of the warm anticyclone over eastern Europe generated northerly

124   winds (Fig. 4). The distinguishing feature of this synoptic process is that it stopped the cyclone over the Black Sea.
125   As a result, the cyclone gained a stationary feature on August 10-12 (Fig. 3c, 3d and 4). The exact mechanism caused
126   floods on July 6-7, 2012, in Krymsk, Novorossiysk, and Glendzhik in the Krasnodar Territory (Alexeevsky et al.,
127   2016). Such abnormal pressure gradient is known to cause prolonged storms and trigger precipitation over very large
128   areas. (Fink et al., 2009). This situation increased the pressure gradient of the surrounding areas with the low pressure
129   developing on the middle parts of the Black Sea (the line between Crimea-Kastamonu), especially since August 10.
130   Thus, the Black Sea gained a vital convergence feature. The activation of the fronts on 09-12 August 2021, the
131   intensification of cyclogenesis on the Black Sea until about 40° latitude, and the presence of active front formation
132   are also noteworthy (Fig. 3a, 3c and 3d). This mechanism was reported on August 22, 2012, as the synoptic mechanism
133   behind the flood disaster in the Tuapse region (Alexeevsky et al., 2016). In addition to all these, the temperature
134   difference between sea surface temperatures and 850 hPa is around 13 °C (Fig. 3e). At 500 hPa, the temperature
135   gradient increased considerably (Fig. 3f). When the relatively cold northerly winds entered the Black Sea, they warmed
136   up from the bottom and the moisture content increased, resulting in an instability condition. In addition to these
137   synoptic processes, physiographic features (elevation, aspect, morphology) also played an important role in
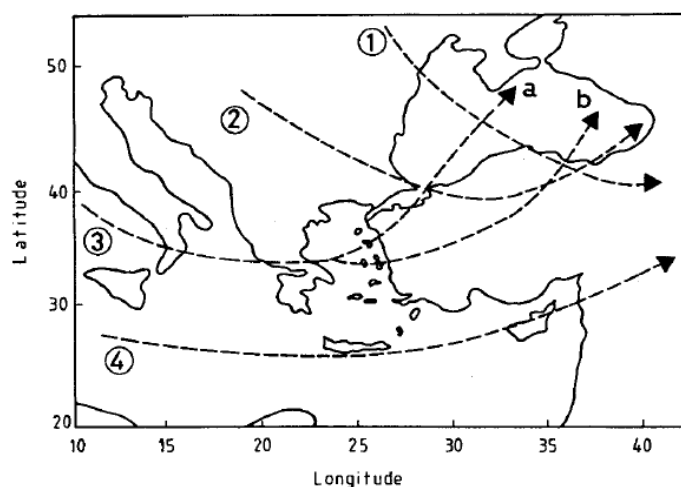138   precipitation variability and values at stations.

139

140   **Figure 2.** The paths of atmospheric cyclones over Turkey from Karaca et al. (2000).

141

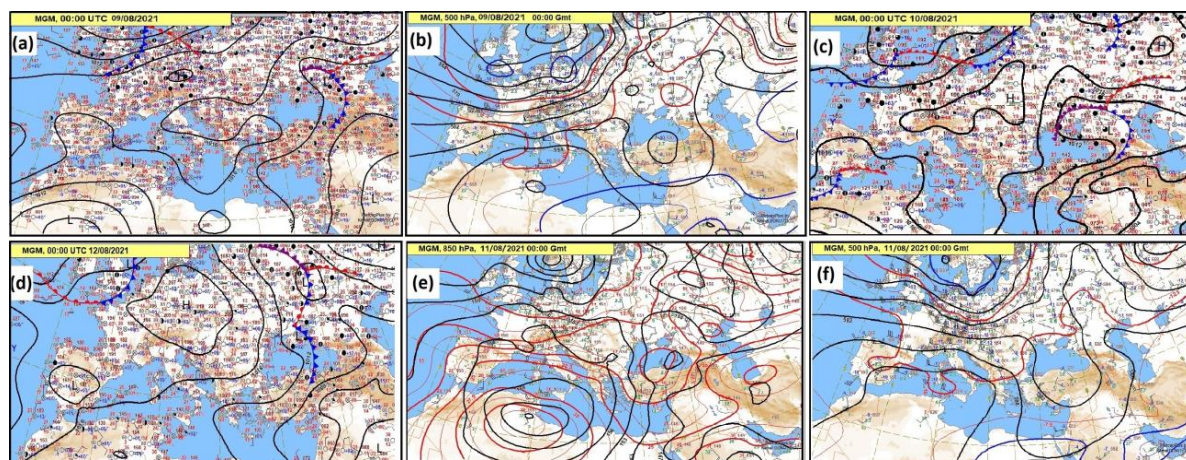**Figure 3.** (**a**) Surface synoptic chart for August 9, 2021. (**b**) Geopotential heights at 500-hPa chart for August 9, 2021. (**c**) Surface synoptic chart for August 10, 2021. (**d**) Surface synoptic chart for August 12 2021. (**e**) 850 hPa synoptic chart for August 11, 2021, and (**f**) Geopotential heights at 500-hPa chart for August 11, 2021. Source: Turkish State Meteorological Service (www.mgm.gov.tr).
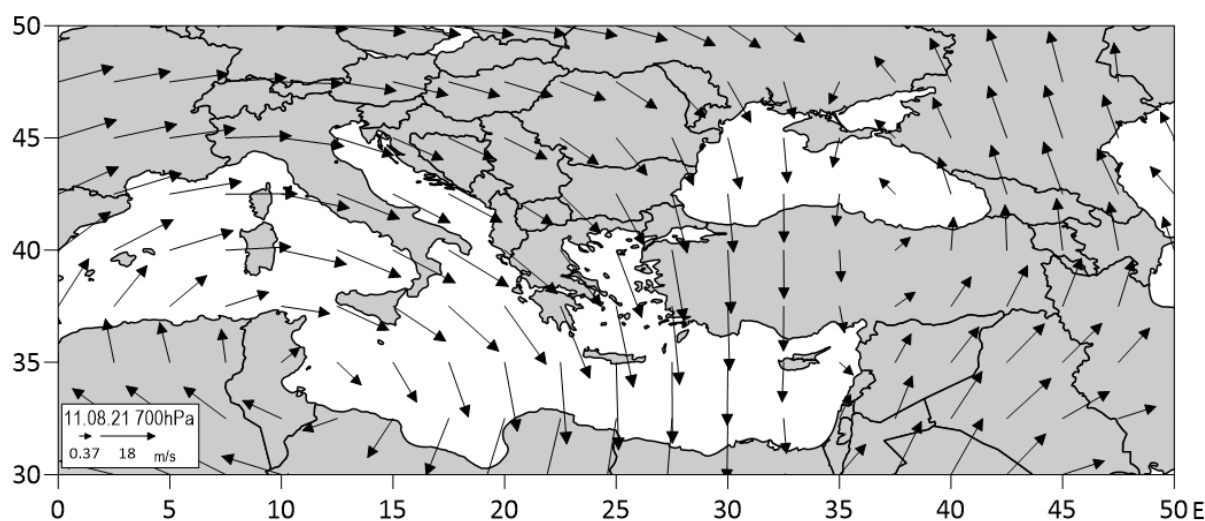

Figure 4. 11 August 2021, 700 hPa wind direction and speed (700 hPa u and v direction vector wind data.).

4.2. Satellite Data

On 10-11-12 August 2021, Natural Color RGB, Day Microphysics RGB, Convection RGB data from Meteosat Second Generation were used to determine the spatial distribution of convective cells and to examine atmospheric conditions. Natural Color RGB uses three solar channel spacings, red (NIR1.6), green (VIS0.8) and blue (VIS0.6). Water clouds with tiny droplets have a considerable reflection in all three channels and therefore appear whitish. Clouds with dense ice particles have a cyan colour and correspond to high clouds (EUMETSAT, 2021) (Figure 5a, 5b, 5c). VIS0.8 IR 3.9 IR 10.8 bands are used in Day Microphysics RGB images. In this way, convection, fog and low-level clouds can be easily observed. This is due to the clouds rising to the troposphere border, especially when the lower layers of the air mass are hot and strong vertical air movement develops. Cold and thick convective clouds with large ice particles on top, e.g. Cb tops, appear red (Figure 5d, 5e, 5f). This is important for detecting rising movements and more severe weather conditions. Another unique situation is that convective clouds are predominantly active when these images are examined in the study area. The Convection RGB combines the brightness temperature difference (BTD) between the WV6.2 and WV7.3 channels (on red), the BTD between the IR3.9 and IR10.8 channels (on green) and the reflectance difference between the NIR1.6 and the VIS0.6 channels (on blue) (EUMETSAT, 2021). Unlike Day Microphysics RGB, convection zones can be observed more easily in Day Convective Storms RGB. Severe convective storms appear bright yellow in this colour scheme (Figure 5g, 5h, 5i). High-level thick ice clouds and convective CB clouds containing large ice crystals appear red, and convective clouds containing tiny ice crystals appear yellow. When the Day Convective Storms RGB images of the Western Black Sea Region are examined, it can be said that convective CB clouds contain tiny ice crystals and strong ascending movements are dominant. (Fig. 5g, 5h and 5i). On August 10-11-12, it is seen that it develops in the north direction and moves southward and exhibits a cyclonic rotation. All these observations showed that precipitation concentrates on the sea and develops convectively. On the other hand, Doğan et al. (2019), according to the simulation results, it is seen that vertical cloud formation and updraft movement disappear as the sea surface temperature decreases. In addition, another result of this model is that it has been concluded that extreme precipitation will lose strength when SST is reduced by 2 °C.
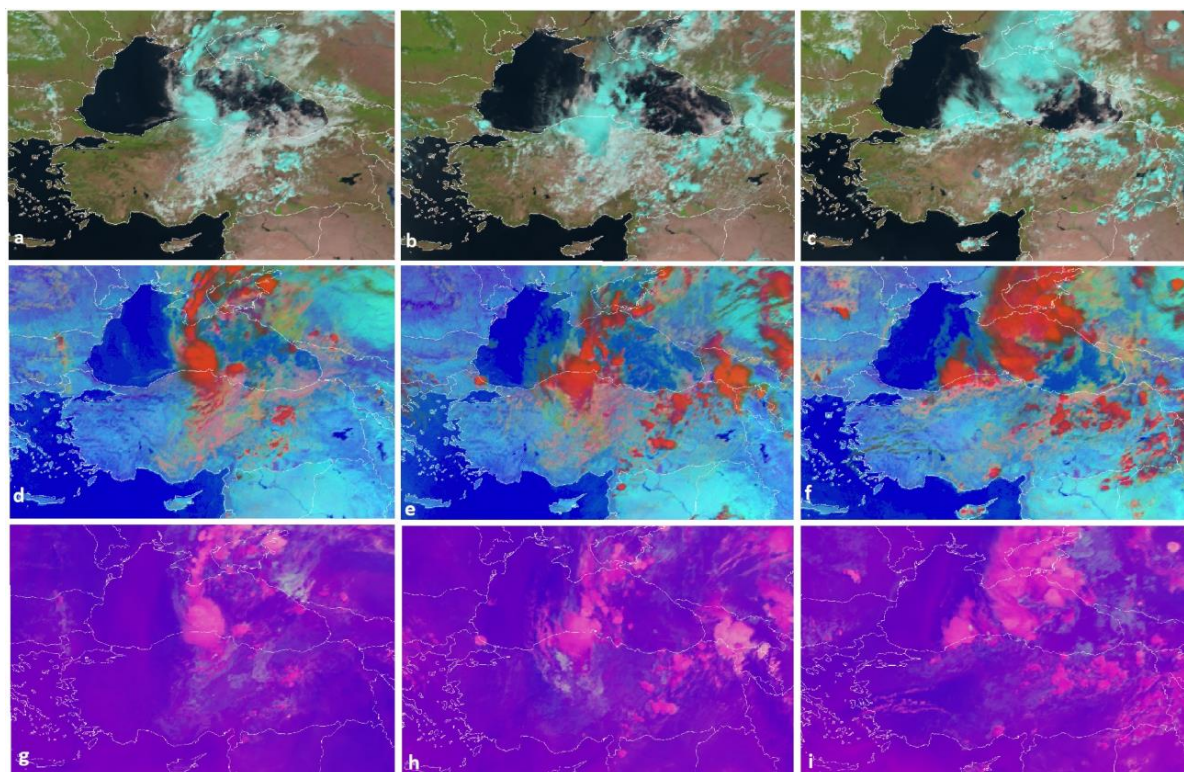
Figure 5. (a, b, c) Satellite images on 10-11-12 August 2021, 10:00 UTC, respectively. Natural Colour RGB product from SEVIRE MSG (Meteosat Second Generation). This satellite product reflects a cyan colour in ice-laden clouds. (d, e, f) Satellite images on 10-11-12 August 2021, 10:00 UTC, respectively. Cold and thick clouds with tops composed of large ice particles appear red. (g, h, i) Satellite images on 10-11-12 August 2021, 10:00 UTC, respectively, indicate severe convective storms. Satellite images on 10-11-12 August 2021, 12:00 UTC, respectively. Source: EUMETSAT (https://www.eumetsat.int/).

4.3. Sea Surface Temperatures

In the Black Sea Basin, some factors play a role in the fact that the average precipitation values on the northern coasts of Turkey do not decrease during the late summer and autumn transitions, especially in the extreme precipitation during these times. These factors should be related to the fact that the surrounding land areas are cooler than the sea, the absorption of solar radiation in the seas is high during these seasons and the landforms. Many studies have proved the effectiveness of seas or lakes on precipitation. For example, Pastor et al. (2001) investigated the relationship between torrential precipitation on the Mediterranean coast of Spain and sea surface temperatures (SST). They determined that SST was a critical factor in developing torrential precipitation in the Western Mediterranean Basin.

191 In the simulations made in Turkey, it is stated that the warm seas increase the precipitation in the Anatolian Peninsula,
192 especially the Black Sea, shows a significant difference in summer when compared to other seas, and the precipitation
193 tends to increase throughout the year with the increase in SST (Bozkurt & Sen, 2011). In our study, where the
194 temperature difference between the sea surface and the upper atmosphere is excellent, many studies emphasize the
195 effect of sea or lakes on precipitation where these temperature differences are emphasized (Suriano & Leathers, 2017).
196 West et al. (2019) pointed out that cloudiness and more precipitation occur over the Sea of Japan when the temperature
197 difference between the sea surface and the level of 850 hPa is 13 °C or more. Especially this mechanism is effective
198 in the west of Japan. Especially in cases where the temperature difference between the surface temperature and 850
199 hPa is 13 °C and above, the lake effect has been accepted as the threshold value for the development of precipitation
200 (Holroyd III, 1971; Kunkel et al., 2002; Niziol, 1987). According to Dai et al. (2018) simulated the lake effect in Nam
201 Co Lake based on data from four meteorological stations from October 2005 to December 2015 on the Tibetan Plateau.
202 They showed that it may have caused an increase of up to 60% in precipitation on the lake and the wind direction (east
203 of the lake) in October. In addition, this study stated that the lake surface was 15.5 °C warmer than the air at 550 hPa
204 in October. This temperature difference increased the instability conditions and caused convections. Wen et al. (2015)
205 examined the effects of Ngoring Lake and Gyaring Lake, which form the source of the Yellow River on the Tibetan
206 Plateau, local temperature and precipitation. It is stated that lakes contribute 49% to the annual precipitation on and
207 around the lake. This contribution is relatively high in the summer months and reaches 72%, especially from July to
208 October. In addition to lakes on the Tibetan Plateau, where similar conditions are experienced, lakes in Boreal regions
209 are also known to increase precipitation in summer (Eerola et al., 2010; Samuelsson et al., 2010). The above references
210 show that although the sea and lake effect is evident in different regions worldwide, the impact time and gradient are
211 significantly different.

212 As in the results of this study, the time interval where the lakes contribute the most to the precipitation around them
213 is night and morning hours when the water is warmer than the land (Fig. 10). In addition to all these, depending on
214 the NOAA data of August 10, 2021, the temperature values of the land areas in the Black Sea basin's surroundings,
215 and the daily minimum temperature values in the coastal areas of Romania, Ukraine, and Russia, Turkey were around
216 21 °C. On the other hand, it decreased to 15 °C in the inner parts where the altitude increased. According to MGM
217 data, this situation dynamically created a breeze of 3 m/s from land to sea due to the increase in the temperature
218 difference between the sea and the land during the night and morning hours. This triggered a low level of horizontal
219 convergence and allowed the air to rise. Thus, the divergence at the upper level contributes to moving the low-level
220 horizontal flow and humidity to the higher level. Thermally, the seas release more latent heat and contribute to
221 evaporation in developing convection for precipitation. This causes instability in the atmosphere.

222   Between 10-17 August 1971-2000, the maximum temperatures were 25 °C, while the minimum temperatures were

223   located northwest of the Black Sea and the Sea of Azov. It is noteworthy that the maximum temperatures between

224   1991 and 2020 exceeded 26 °C. In the sea surface temperatures of 10-17 August 2021, a temperature above 28 °C in

225   the east of the Black Sea is remarkable (fig. 6). There was a temperature anomaly of 3.5 °C in areas where convective

226   cells developed on days with extreme precipitation. As a source of evaporation, the warm sea in the north of the study

227   area has an essential effect on precipitation. In particular, it exceeded 27 °C in the central part of the Black Sea and

228   28 °C in the eastern part of August 10, 2021, SST (Fig. 6).

229   On the other hand, as seen in Fig. 6, the temperatures of the sections mentioned on August 13 decreased, and the hot

230   sections narrowed. This date is essential because it is the date when extreme precipitation ends. Especially in the south

231   of the Sea of Azov, where the convective cell developed, temperatures dropped to 25 °C on August 14 and 23 °C on

232   August 17. As a result of the evaporation of the water, the temperature was transferred from the sea surface to the

233   atmosphere, and the warm air was raised by convection. This situation continued between 10 and 13 August. The

234   south of the Azov Sea, about 27 °C before the start of precipitation, dropped to 23 °C on August 17, creating a

235   temperature difference of 5 degrees. As a result of such excessive precipitation, temperature differences of 3-5 °C

236   occur on the sea surfaces (Pastor et al., 2001). Another well-known result is the deepening of the low-pressure centre

237   as sea surface temperatures increase in the Eastern Black Sea Region (Doğan et al., 2019). This event is vital in

238   explaining both the role of the Black Sea and the source of excessive precipitation.
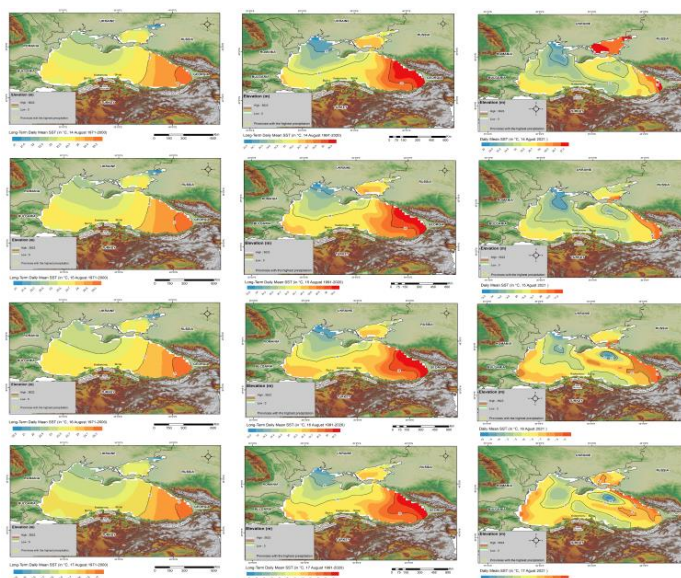

239
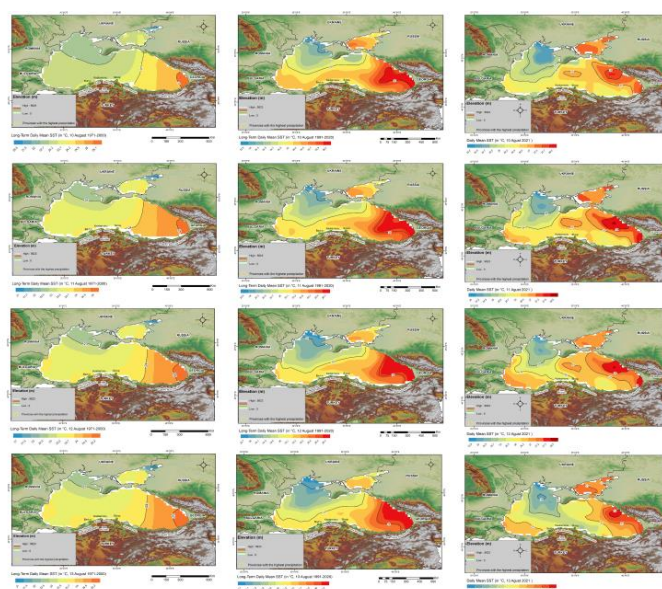
Figure 6. The first column is 10-17 August 1971-2000 SST; the Second column is 10-17 August 1991-2020 SST, and the third column is 10-17 August 2021 SST, respectively.

4.4. Physiographic Conditions

In often mountainous regions where the precipitation gradient is complex and station distributions are not sufficient, it is crucial to understand the influence of topography in order to be able to interpolate precipitation spatially (Johansson & Chen, 2003). Mountains that cut the general circulation vertically cause orographic precipitation by forcing mobile depressions and front systems to rise, while precipitation tends to decrease depending on the height of the mountain on leeward slopes (Gönençgil, 2009; Smith, 1979). Studies conducted in this context show that the precipitation intensity also increases depending on the speed of forcing the air parcel to rise and the slope of the mountain (Smith, 1979; Weston & Roy, 1994). For example, on November 3, 1987, 817 mm of precipitation was measured in the Gulf of Valencia within 24 hours. In the same region, in the storm in October 1982, 632 mm of precipitation was measured in 24 hours. The common feature of these precipitations is that the moist air coming from the sea is channelled into the valleys and forced to rise. While these extreme precipitations created a flood, the extreme precipitation experienced in October 1982 caused the collapse of the Tous dam (Peñarrocha et al., 2002). Therefore, physiographic conditions are of great importance in extreme precipitation. In order to better evaluate the extreme conditions in the study area, daily precipitation data of a total of 56 stations located in Sinop, Kastamonu and Bartın were used. The number and distribution of stations are sufficient spatial resolution and reflect the orographic effect.

258   Considering the total precipitation distribution of 45 stations located on the northern and southern slopes of the Küre
259   Mountains, which exhibit an east-west directional orographic barrier in the study area, it was observed that there were
260   differences in extreme precipitation values (Fig. 7). In the total precipitation distribution of 45 stations between 10-12
261   August, it can be seen that the highest precipitation is located on the northern slopes and decreases on the southern
262   slopes as one move towards the interior (Fig. 7). 3-day precipitation totals to understand the topographical effect were
263   listed according to the altitude and aspect conditions of the stations. It can be clearly stated that the air masses
264   channelled into the valleys and forced to orographic uplift quickly create adequate precipitation. For this situation, a
265   terrain model was made to show the orographic effect at stations 19030 (Devrakani/Kuzköy) and 19032
266   (Bozkurt/Mamatlar Village) located around the Ezine Stream, where the flood was experienced and where the
267   maximum rainfall was recorded (Fig 8). The black arrows on the model, representing the winds, are based on the wind
268   directions of the times when MGM is measuring, and the maximum hourly precipitation is seen (Fig. 7). For example,
269   the total precipitation values measured in Devrakani/kuzköy and Bozkurt/Mamatlar were three times higher than the
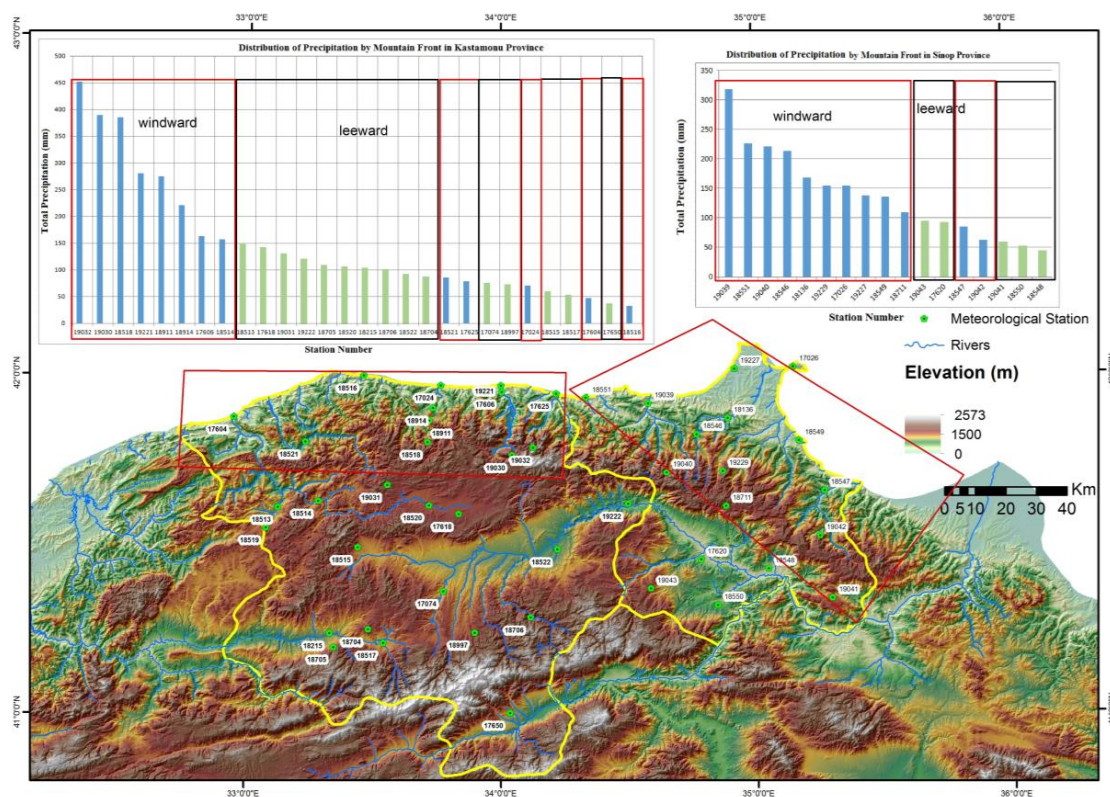270   sum of the extreme values measured at the coastal stations.

Figure 7. Distribution of 45 stations to reflect the orographic effect. The red boxes roughly represent the northern slopes (winward). The stations that are distributed outside the box are the leeward stations behind the orographic barrier. In addition, the total precipitation of these stations on 10-12 August is shown with a column chart.
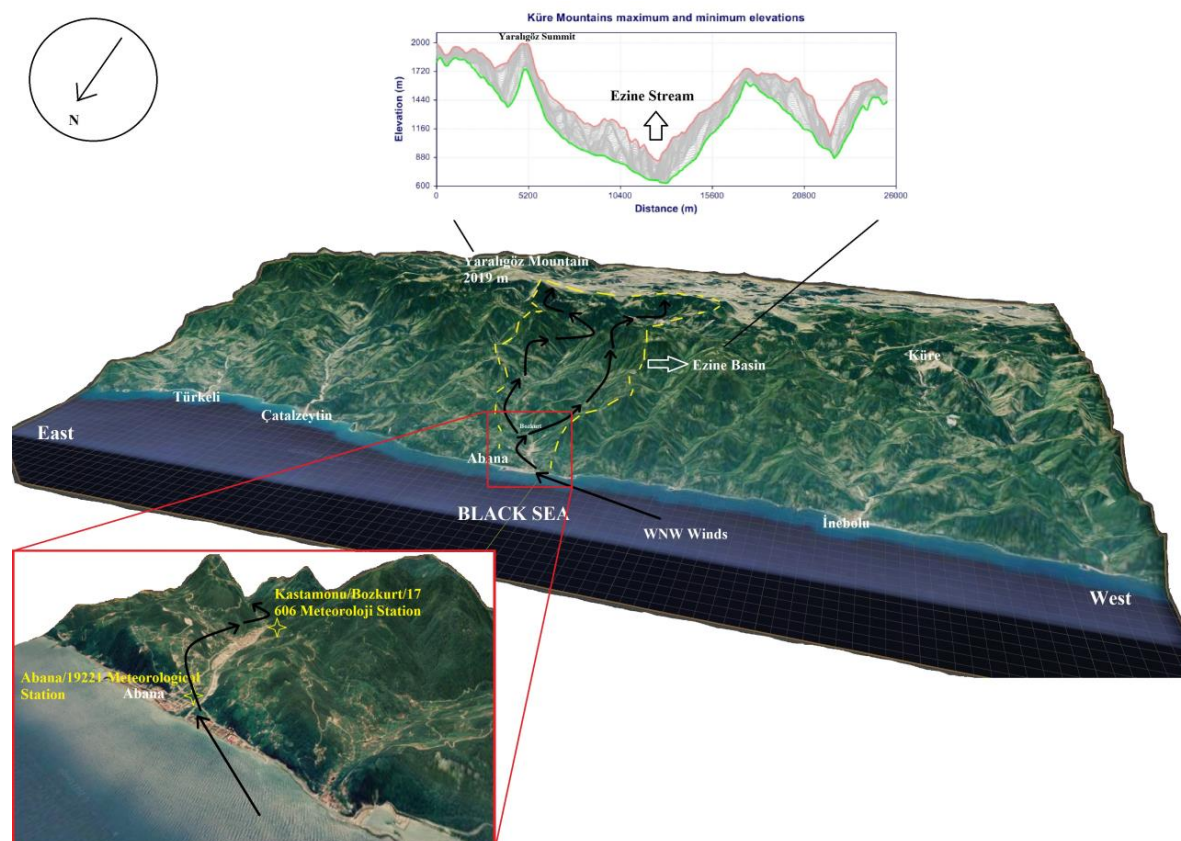
Natural Hazards
and Earth System
Sciences

Discussions

Figure 8. Elevation profile (maximum and minimum) of the northern slopes of the Küre Mountains, where the maximum precipitation was measured. 19030 (Devrakani/Kuzköy) and 19032 (Bozkurt/Mamatlar Village) stations are located on the northern slopes of Yaralıgöz Hill at an altitude of 1500 meters. Arrows represent the prevailing wind direction of Abana Meteorology station and Kastamonu Bozkurt station on August 11 (From © Google Maps and SRTM data via BlenderGIS).

On August 11, the cold air coming from the northwest of the Black Sea Basin moved from west to east, following the morphology of the coastline. To the east of Sinop, the air mass turned north and moved towards the cyclone's centre. Wind directions were west, northwest and west-northwest along the coastline in Amasra, Kurucaşile, İnebolu, Abana, Çatalzeytin and Türkeli between 08:00 - 09:00 UTC. Winds in this direction can quickly move from the mouths of the valleys to the interior of the land. The maximum precipitation falling in the region on August 11 was in the coastal line from Bartın to the east of Sinop and the N-S directional valleys. Maximum hourly precipitation measurements observed between 08:00 and 10:00 in Bozkurt/Mamatlar and Devrakani/Kuzköy are closely related to this situation (Fig. 9).
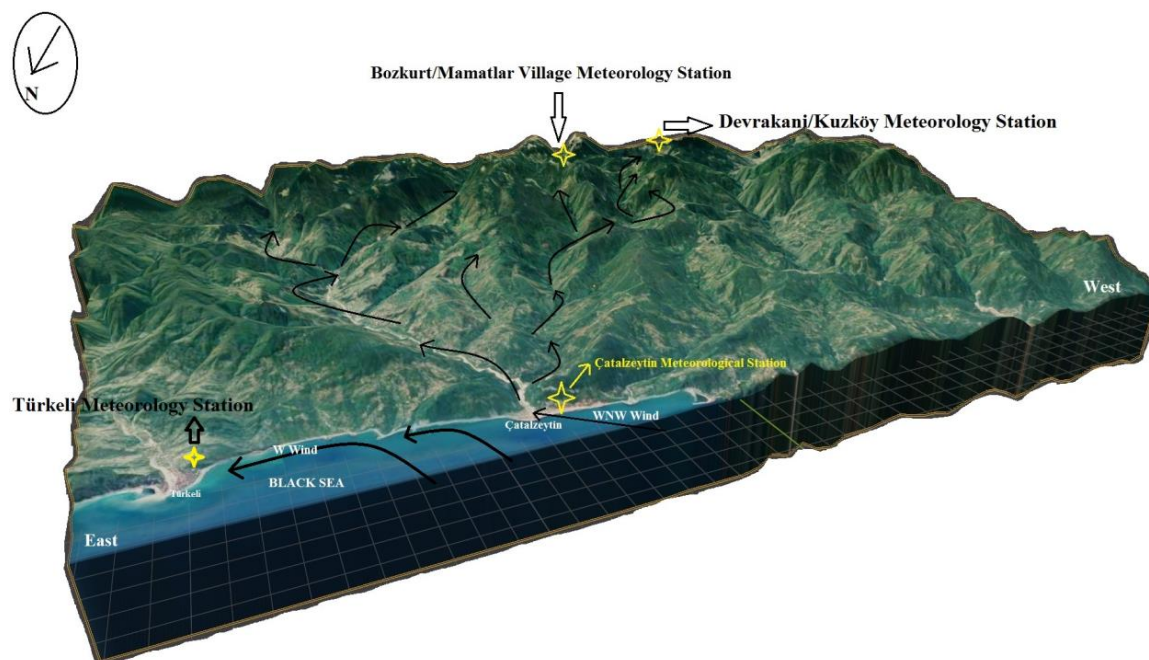
16

Figure 9. Arrows represent west-northwest winds for Türkeli and Çatalzeytin stations between 08:00 and 09:00 UTC on August 11. 61 mm of precipitation was measured in Turkeli on August 11 at 09:00 UTC. Wind data could not be measured in Bozkurt Mamatlar and Devrekani Kuzköy for these dates, and in terms of channelling into valleys, north for Mamatlar station and predominantly east and northeast winds for Devrekani Kuzköy must have been effective (From © Google Maps and SRTM data via BlenderGIS).

4.5. Extreme Precipitation Analysis

For the extreme precipitation analysis, hourly precipitation was first evaluated, and then daily evaluations were made. Precipitation intensity was calculated from hourly data and evaluated according to five rainfall intensity classes recommended by MGM (Table 2). The highest hourly precipitation in the study area was measured on August 11. Hourly precipitation values measured between 06:00 and 09:00 UTC on August 11 in Bozkurt/Mamatlar were over 45 mm and are defined as heavy precipitation according to the precipitation intensity class. The precipitation measured at 10:00 at this station corresponds to extreme precipitation. Devrakani/Kuzköy meteorological station showed similar values and reached 60 mm, especially at 09:00 UTC. In terms of hourly extremes, 70 mm of precipitation was measured one hour (on August 10, 22:00 UTC) at Ulus/Ceyüpler station (Fig. 10). This value is very close to the heavy rainfall threshold value.

304   **Table 2:** Precipitation intensity classification according to MGM.

Precipitation Intensity	Hourly Rainfall Amount
Light precipitation	1- 5 mm
Moderate Precipitation	6- 20 mm
heavy Precipitation	21- 50 mm
Very Heavy Precipitation	51- 75 mm
violent Precipitation	76-100 mm
Excessive precipitation	Over 100 mm

305   In order to determine the precipitation intensity levels suitable for the conditions of Turkey, different precipitation
306   amounts and severity levels were separated in various climatological studies (Ardel et al., 1969; Çiçek, 2001; Dönmez,
307   1990; Koçman, 1993). In this study, a different classification was used in order to provide the opportunity to evaluate
308   all the precipitations of more than a specific value. Thus, with the IDW (Inverse distance weighting) interpolation
309   method, the daily measured precipitation for 10, 11 and 12 August and then the total precipitation for today were
310   mapped (Fig 11, 12 and 13). In the Black Sea precipitation regime, daily maximum precipitation values of 431.5 mm
311   in Zonguldak and 240.9 mm in Rize have been measured (Koçman, 1993). However, on August 11, 2021, 297.4 mm
312   of daily precipitation was measured for Kastamonu province. As a result of the precipitation that continued for three
313   days, 452, 318 and 236 mm precipitation were measured in the Kastamonu, Bartın and Sinop provinces, respectively.
314   These provinces are among the highest measured values to date. (Figures 11, 12 and 13). In addition, the precipitation
315   in Bartın province was represented with the highest values in this regime as hourly precipitation according to the
316   MGM records. Flooding occurred in these three provinces due to excessive rainfall. Especially in Kastamonu-Bozkurt,
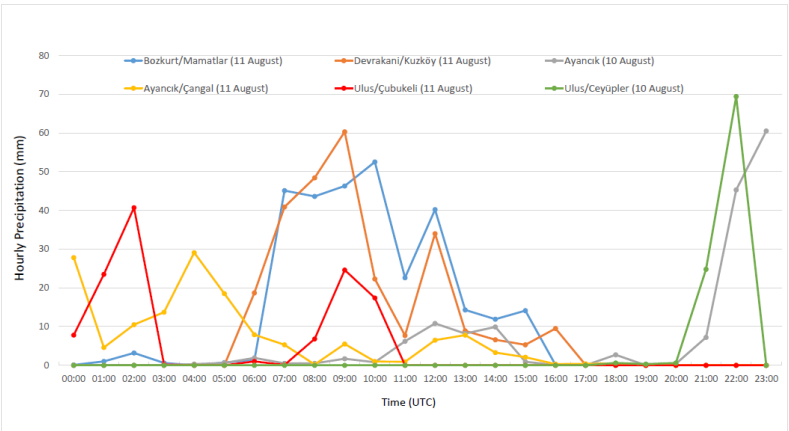317   the settlements in the valley brought great losses (Fig.16).

318

Figure 10. Hourly precipitation measurements for August 10-11, 2021.
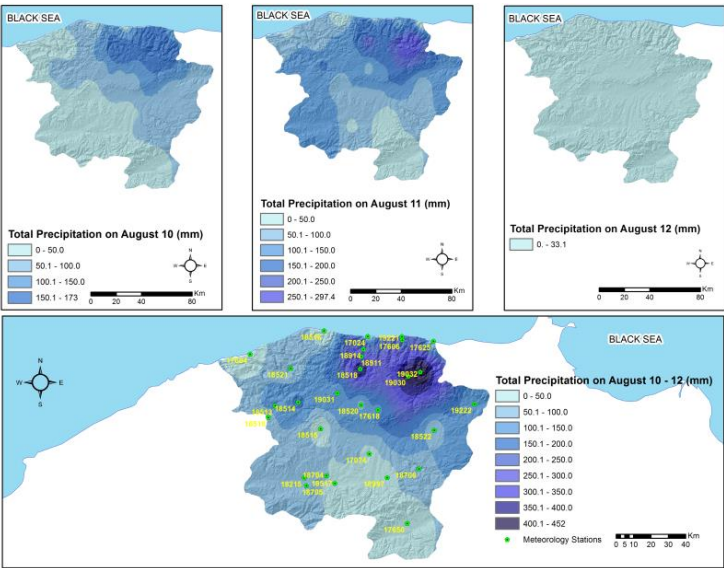

Figure 11. The daily precipitation distribution of the province of Kastamonu on 10-12 August.
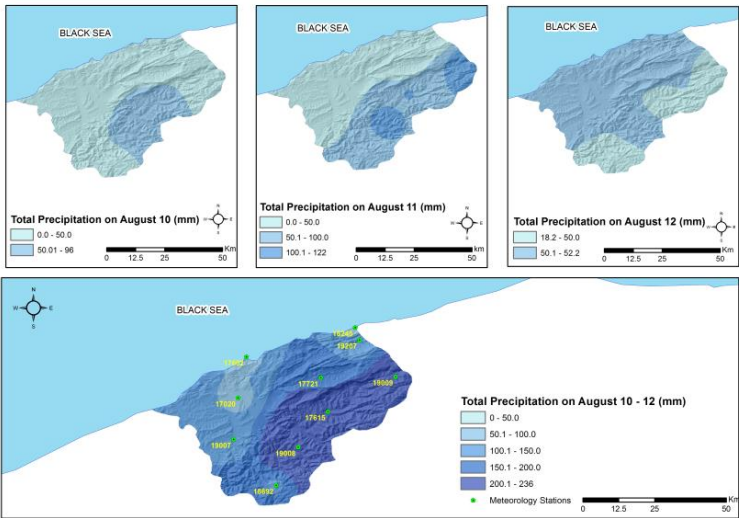

Figure 12. The daily precipitation distribution of the province of Bartın on 10-12 August.
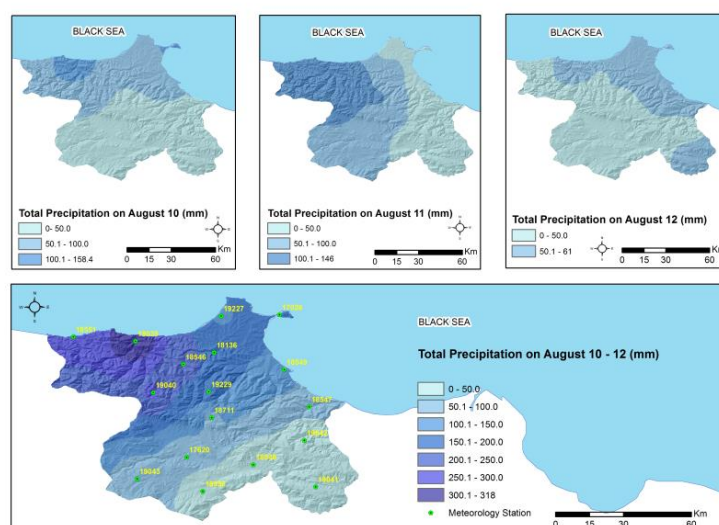
325

326 **Figure 13**. The daily precipitation distribution of the province of Bartın on 10-12 August.

327 **4.5.1. Wind Analysis**

328 During the dates of extreme precipitation, the dominant wind direction mainly was W-N-NW direction winds to the
329 atmospheric conditions of that day. Precipitation increased during the hours when the warm and humid northern winds
330 over the Black Sea were effective. On the contrary, the other important wind direction during the hours of extreme
331 precipitation was southerly winds. According to the daily temperature data obtained from NOAA, on August 10, 2021,
332 the minimum temperature was 15.2, the maximum temperature was 28.4, and the average temperature was 25.6 °C at
333 Kastamonu Meteorology Station. Especially after noon, the temperature dropped to 17°C. On August 11, 2021, the
334 maximum temperature was measured at 18 degrees. These values are also supported by the SEVIRE MSG data with
335 synoptic observation (Figures 14a, 14b and 14c). The temperature on the coasts of Sinop was 24 °C. These temperature
336 values reached lower on August 12, 2021 (Figure 14c). During these dates, the temperature difference between the
337 land and the sea approached 10 °C. As a result, a clear contrast has occurred in the meteorological elements in a short
338 period, which is expressed as discontinuity. This situation must have triggered the southerly winds. This must have
339 affected the relatively warm and humid air coming from the north and the colder and drier air to meet each other
340 mainly channelled into the valleys. As a result, extreme precipitation was recorded during the hour intervals when the
341 southerly winds blew (Figure 15). Previous studies have determined that this mechanism effectively causes excessive
342 precipitation on the Eastern Black Sea coast (Baltaci, 2017).
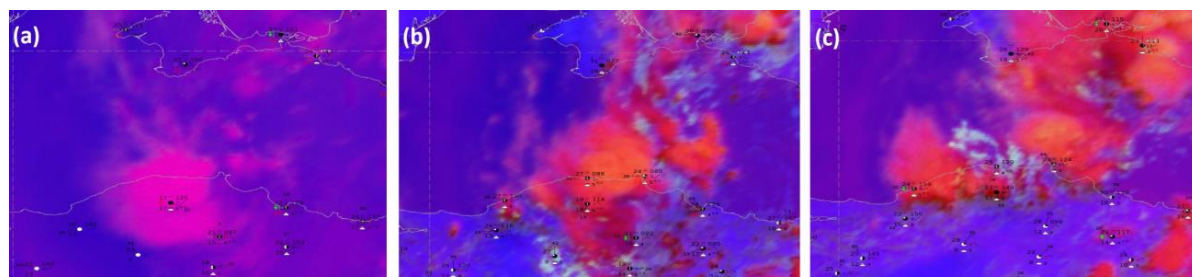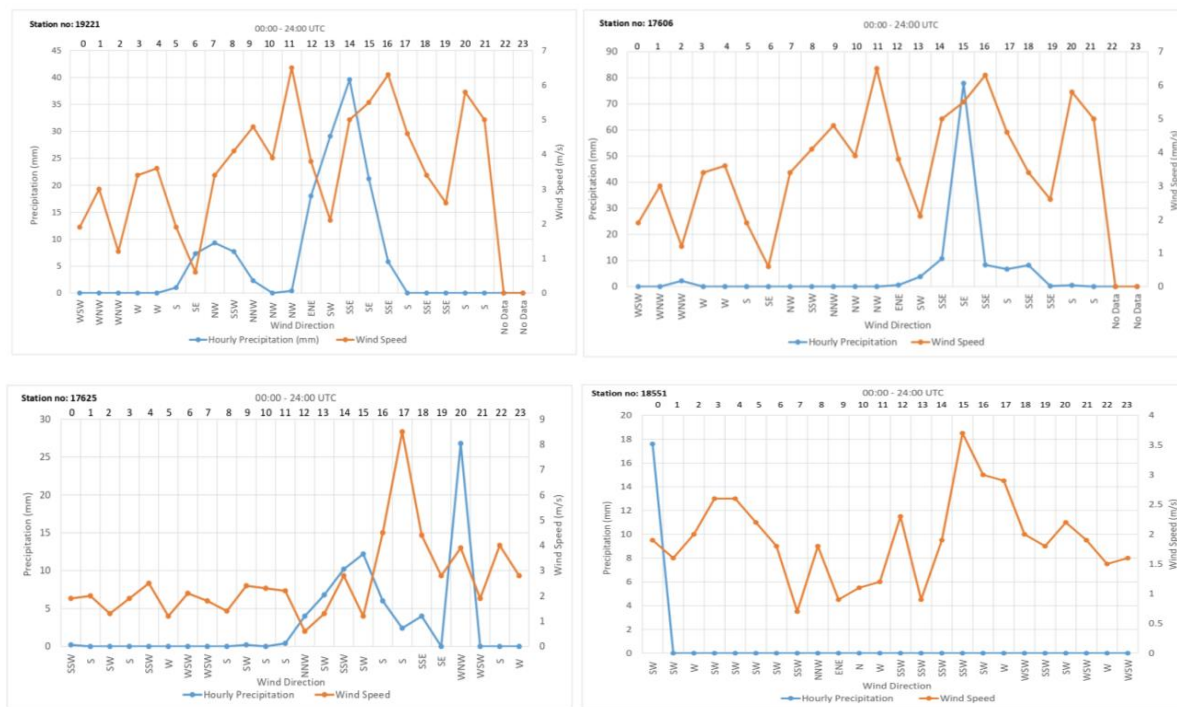
343

Figure 14. (a) Convection RGB product from SEVIRE MSG (Meteosat Second Generation) together with SYNOP observations, 2021-08-10 18:00Z. (b) 2021-08-10 12:00Z. (c) 2021-08-12 12:00Z. Source: EUMETSAT (https://www.eumetsat.int/).
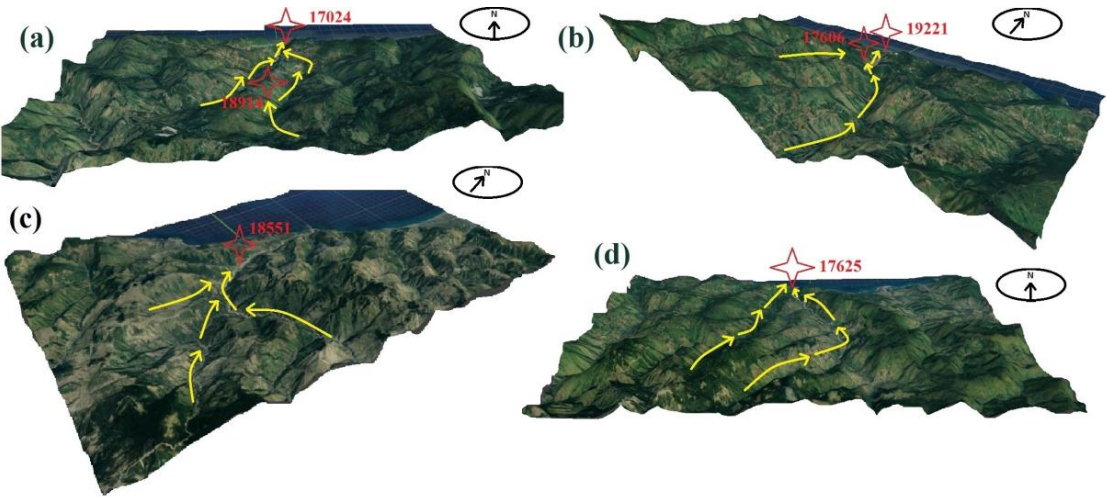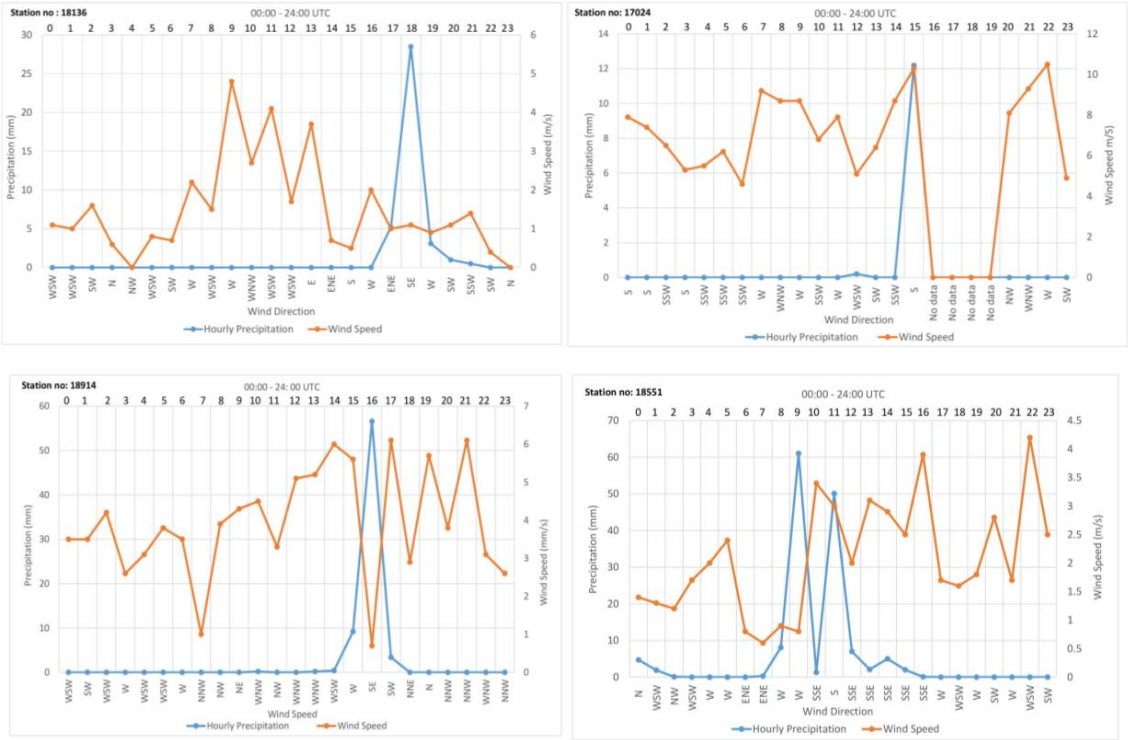
346

347

348

349

350

351

Figure 15. Hourly south winds and hourly precipitation values with station numbers. (a) Winds from the south for station 17024 and southeasterly for station 18914. (b) Southeasterly winds for both stations 17606 and 19221. (c) For station 18551, the winds

354 blew in line with the southwest-trending valley. (d) Southwest and southeast oriented valleys for station 17625 (From © Google Maps
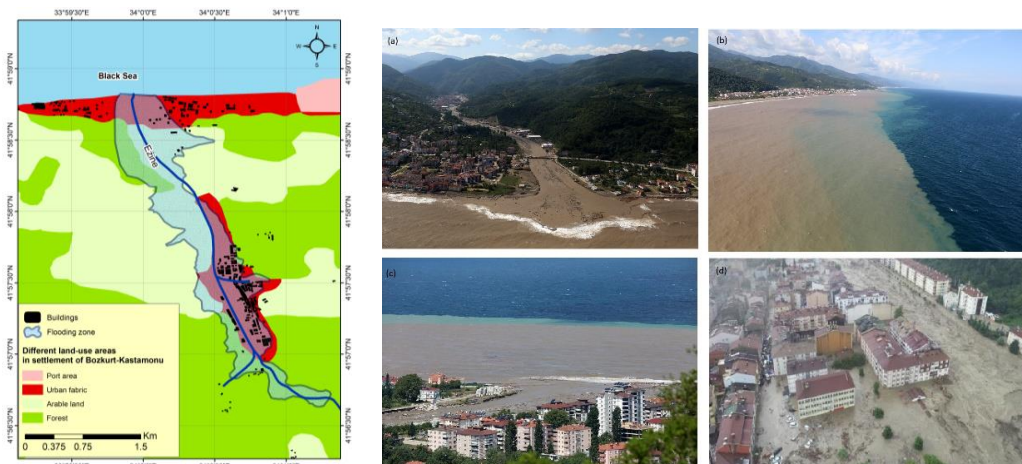355 and SRTM data via BlenderGIS).

356

357 **Figure 16.** Different land use and buildings within the floodplain. Ezine Stream, Bozkurt. Photos showing the destructive effects
358 of the 11 August 2021 flash floods: (a) The mouth of the Ezine Valley and the entrance of the suspended loads to the Black Sea,
359 (b and c) progress of suspended loads in the Black Sea, (d) floodplain. Represents the largest flood in the three provinces,
360 experienced August 10-12, 2021 (https://www.afad.gov.tr/bartin-kastamonu-ve-sinopta-). Photos source: www.ensonhaber.com.

361 **5 Conclusion**

362 In this study, the synoptic conditions of extreme precipitation in the provinces of Sinop, Kastamonu and Bartın were
363 investigated. As a result of the heavy rains that fell on these provinces in three days, Bartın Ulus; Kastamonu Azdavay,
364 İnebolu, Bozkurt, Küre and Pınarbaşı districts and Sinop Ayancık districts were affected by the flood. According to
365 the official figures included in the Turkey Ministry of Interior Disaster and Emergency Management Presidency
366 (AFAD) on 01.09.2021, 82 people (71 in Kastamonu, 10 in Sinop, and 1 in Bartın) lost their lives due to the flood. In
367 addition, energy, transportation, access to drinking water, communication and shelter areas were damaged by the
368 flood.

369 When the synoptic conditions were examined, the high-pressure area moved eastward over Europe on August 10 and
370 was located northwest and northeast of the Black Sea. The blocking presence of the warm anticyclone over eastern
371 Europe generated north-northeast winds. The distinguishing feature of this synoptic process is that it stopped its
372 cyclone over the Black Sea. Because the blocking feature of the static high pressure in the area blocked the roads of
373 the cyclone to the north and northeast. Since August 10, the pressure gradient of the surrounding areas has increased

374 with the low pressure developing in the middle parts of the Black Sea (the line between Crimea and Kastamonu). The
375 activation of the fronts on 10-12 August 2021, the intensification of cyclogenesis on the Black Sea until about 40°
376 latitude, and the presence of active front formation are also noteworthy. In areas where this low pressure was located
377 on the Black Sea, the effectiveness of the cyclone increased, with the SST being 27 °C. Thus, the Black Sea gained a
378 strong low-level convergence feature. In addition to all these, the temperature difference between the sea surface and
379 850 hPa reached 13 °C. The cold air, which entered the Black Sea from the north-northwest, warmed while moving
380 towards the low-pressure centre on the Black Sea, moved along the northern coast of Turkey, oriented towards the
381 Kerch Strait and gained a cyclonic characteristic. As a result of this action, the heated air mass also encountered the
382 cold air coming over the Turkish lands, increasing the instability conditions and heavy rains were also influential. In
383 particular, topographic conditions affected the spatial distribution of excessive precipitation.

384 It is an atmospheric situation that can be expected to experience more such events triggered by the differentiation in
385 sea-land surface temperatures, with the temperature increases predicted in the coming years. In this context, heavy
386 rains are expected to increase in the coming years. Applicable plans should be made to protect residential areas from
387 damage caused by heavy rainfall events. Preventing construction around the floodplains of rivers, especially in areas
388 where floods and flood disasters have occurred in the past, and revising the zoning plans according to the changing
389 climatic conditions are among the most critical requirements. In addition, to create a sustainable, healthy, smart and
390 resilient local society, the residents have to be educated about the risk of disasters, climate adaption and action.

391 *Author contribution.* O.H prepared the article with contributions from all co-authors. B.G developed the idea for the
392 article. The B.G and Z.A checked the content of the article and gave necessary directions (methodology, reviewing,
393 editing of the manuscript). In addition, Z.A produced the 700 hPa wind direction map. All remaining figures and maps
394 were produced by O.H.

395 *Data availability.* The following data sets are publicly available. Synoptic charts of the daily event are available at
396 https://mgm.gov.tr/sondurum/guncel-haritalar.aspx. Sea surface temperature data are available at
397 https://psl.noaa.gov/data/gridded/data.noaa.oisst.v2.highres.html. The satellite data used for the case study are
398 available at http://www.eumetrain.org/ and https://view.eumetsat.int/productviewer?v=default. Additionally, daily
399 temperature data is available at https://www.ncei.noaa.gov/maps/daily-summaries/ and August 11, 2021, 700 hPa u
400 and v direction vector wind data available at https://psl.noaa.gov/data/gridded/data.ncep.reanalysis.html. Land use
401 data are available at https://land.copernicus.eu/pan-european/corine-land-cover/clc2018?tab=download. You can
402 contact the responsible author about other data you are interested in.

403 *Competing interests.* The authors declare that there is no conflict of interest.

Natural Hazards
and Earth System
Sciences
Discussions

404
405
406
407
408   **References**
409
410   Alexeevsky, N., Magritsky, D. V., Koltermann, K. P., Krylenko, I., and Toropov, P.: Causes and systematics of
411   inundations of the Krasnodar territory on the Russian Black Sea coast, Nat. Hazards Earth Syst. Sci., 16,
412   1289–1308, https://doi.org/10.5194/nhess-16-1289-2016, 2016.
413   AFAD.: Bartın, Kastamonu ve Sinop'ta meydana gelen yağışlar hakkında,
414   Ardel, A., Kurter, A., ve Dönmez, Y.: Klimatoloji Tatbikatı, İstanbul Üniversitesi Yayınları, 1123, Edebiyat
415   Fakültesi Coğrafya Enstitüsü Yayınları 40, İstanbul, 1969.
416   Baltaci, H.: Meteorological analysis of flash floods in Artvin (NE Turkey) on 24 August 2015, Nat. Hazards Earth
417   Syst. Sci., 17, 1221–1230, https://doi.org/10.5194/nhess-17-1221-2017, 2017.
418   Bocheva, L., Marinova, T., Simeonov, P., and Gospodinov, I.: Variability and trends of extreme precipitation events
419   over Bulgaria (1961-2005). Atmos. Res. 93, 490-497. https://doi.org/10.1016/j.atmosres.2008.10.025, 2009.
420   Bozkurt, D. and Sen, O. L.: Precipitation in the Anatolian Peninsula: sensitivity to increased SSTs in the surrounding
421   seas, Clim. Dynam., 36, 711–726, https://doi.org/10.1007/s00382-009-0651-3, 2011.
422   Çiçek, İ.: Türkiye'de günlük yağış şiddetleri ve frekansları, Ankara Üni. Türkiye Coğraf. Araş. Uyg. Mer. Derg. 8,
423   27-48, Ankara, 2001.
424   Dai, Y., Wang, L., Yao, T., Li, X., Zhu, L., & Zhang, X.: Observed and simulated lake effect precipitation over the
425   Tibetan Plateau: an initial study at Nam Co Lake, J. Geophy. Res.: Atmos. 123, 6746-6759, 2018.
426   Doğan, O. H., Önol, B., Turunçoğlu, U. U., and Kahraman, A.: Heavy Precipitation Sensitivity of Sea Surface
427   Temperature over the Eastern Blacksea Region: Ensemble Simulations of Hopa / Artvin Case, in 9th
428   International Symposium on Atmospheric Sciences (ATMOS 2019), ITU, Istanbul, 23 October 2019, 614-
429   618, 2019.
430   Dönmez, Y.: Umumi klimatoloji ve İklim Çalışmaları, İstanbul Üniversitesi, İstanbul, 1990.
431   Eerola, K., Rontu, L., Kourzeneva, E., and Shcherbak, E.: A study on effects of lake temperature and ice cover in
432   HIRLAM, Boreal Environ Res. 15, 130–142, 2010.
433   Erinç, S.: Klimatoloji ve Metodları (4. Baskı), İstanbul, 1996.
434   Erol, O.: Genel Klimatoloji, Çantay Kitabevi (9.Baskı), İstanbul, 2011.
435   Fink, A. H., Brücher, T., Ermert, V., Krüger, A., and Pinto, J. G.: The European storm Kyrill in January 2007: synoptic
436   evolution, meteorological impacts and some considerations with respect to climate change, Nat. Hazards
437   Earth Syst. Sci., 9, 405–423, https://doi.org/10.5194/nhess-9-405-2009, 2009.
438   Gönençgil, B.: Küresel Degradasyon Sürecinde Dağlar ve Dağ Alanları Yönetimi, Çantay Yayınları, İstanbul, 2009.
439   Holroyd III, E. W.: Lake-effect cloud bands as seen from weather satellites. J. of Atmos. Sci., 28, 1165-1170,
440   https://doi.org/10.1175/1520-0469(1971)028<1165:LECBAS>2.0.CO;2, 1971.
441   Johansson, B. and D. Chen (2003). "The influence of wind and topography on precipitation distribution in Sweden:
442   Statistical analysis and modelling." International Journal of Climatology: A Journal of the Royal
443   Meteorological Society 23(12): 1523-1535.
444   Kapochkina, A., Kapochkin, B., Kucherenko, N., and Uchytel, I.: Floods and droughts as a result of deformability of
445   the geological environment, Meteor. Hydrol. Water Manage., 3, 3-7, https://doi.org/10.26491/mhwm/58810,
446   2015.
447   Karaca, M., Deniz, A., and Tayanç, M.: Cyclone track variability over Turkey in association with regional climate,
448   Int. J. Climatol., 20, 1225-1236. https://doi.org/10.1002/1097-   0088(200008)20:10<1225::AID-
449   JOC535>3.0.CO;2-1, 2000.
450   Katz, R. W., and Brown, B. G.: Extreme events in a changing climate: Variability is more important than averages.
451   Climatic change, 21, 289-302, https://doi.org/10.1007/BF00139728, 1992.
452   Koçman, A.: Türkiye İklimi, Ege Universitesi, İzmir, 1993.

Natural Hazards
and Earth System
Sciences
Discussions

Open Access

EGU

453 Korshenko, E., Zhurbas, V., Osadchiev, A., and Belyakova, P.: Fate of river-borne floating litter during the flooding
454   event in the northeastern part of the Black Sea in October 2018, Marine Poll. Bull., 160, 111678,
455   https://doi.org/10.1016/j.marpolbul.2020.111678, 2020.
456 Kunkel, K. E., Westcott, N. E., and Kristovich, D. A.: Assessment of potential effects of climate change on heavy
457   lake-effect snowstorms near Lake Erie, J. Great Lakes Res. 28, 521-536. https://doi.org/10.1016/S0380-
458   1330(02)70603-5, 2017.
459 Niziol, T. A.: Operational forecasting of lake effect snowfall in western and central New York, Weather Forecasting
460   2, 310-321, https://doi.org/10.1175/1520-0434(1987)002<0310:OFOLES>2.0.CO;2, 1987.
461 Pastor, F., Estrela, M. J., Peñarrocha, D., and Millán, M. M.: Torrential rains on the Spanish Mediterranean coast:
462   Modeling the effects of the sea surface temperature. J. App. Meteorol. 40, 1180-1195.
463   https://doi.org/10.1175/1520-0450(2001)040<1180:TROTSM>2.0.CO;2, 2001.
464 Peñarrocha, D., Estrela, M. J., and Millán, M.: Classification of daily rainfall patterns in a Mediterranean area with
465   extreme intensity levels: the Valencia region, Int. J. Climatol.: A J. Royal Meteorol. Soc. 22, 677-695, 2002.
466 Reynolds, R.W., Smith, T. M., Liu, C., Chelton, D. B., Casey, K. S., and Schlax, M. G.: Daily high-resolution-blended
467   analyses for sea surface temperature, J. Climate, 20, 5473–5496, https://doi.org/10.1175/2007JCLI1824.1,
468   2007.
469 Samuelsson, P., Kourzeneva, E., and Mironov, D.: The impact of lakes on the European climate as simulated by a
470   regional climate model, Boreal Environ Res. 15, 113-129, 2010.
471 Smith, R. B.: The influence of mountains on the atmosphere. Adv. Geophy, 21, 87-230
472   https://doi.org/10.1016/S0065-2687(08)60262-9, 1979.
473 Suriano, Z. J. and D. J. Leathers.: Synoptic climatology of lake-effect snowfall conditions in the eastern Great Lakes
474   region, Int. J. Climatol., 37, 4377-4389, https://doi.org/10.1002/joc.5093, 2017.
475 Wen, L., Lv, S., Li, Z., Zhao, L., and Nagabhatla, N.: Impacts of the two biggest lakes on local temperature and
476   precipitation in the Yellow River source region of the Tibetan Plateau, Adv. Meteorol. 2015,
477   https://doi.org/10.1155/2015/248031, 2015.
478 West, T. K., Steenburgh, W. J., and Mace, G. G.: Characteristics of sea-effect clouds and precipitation over the Sea
479   of Japan region as observed by A-Train satellites. J. Geophy. Res.: Atmos., 124, 1322-1335,
480   https://doi.org/10.1029/2018JD029586, 2019.
481 Weston, K. J., and M. G. Roy.: The directional-dependence of the enhancement of rainfall over complex orography,
482   Meteorol. App. 1, 267-275, https://doi.org/10.1002/met.5060010308, 1994.
483 Yüksek, Ö., Kankal, M., and Üçüncü, O.: Assessment of big floods in the Eastern Black Sea Basin of Turkey, Environ.
484   Monit. Assess., 185, 797-814, https://doi.org/10.1007/s10661-012-2592-2, 2013.
485
486
487
488
489
490
491
492
493
494
495
496
497
498